

## CONDENSED MATTER PHYSICS

## Readout and control of the spin-orbit states of two coupled acceptor atoms in a silicon transistor

Joost van der Heijden<sup>1</sup>, Takashi Kobayashi<sup>1</sup>, Matthew G. House<sup>1</sup>, Joe Salfi<sup>1</sup>, Sylvain Barraud<sup>2</sup>, Romain Laviéville<sup>2</sup>, Michelle Y. Simmons<sup>1</sup>, Sven Rogge<sup>1\*</sup>

Coupling spin qubits to electric fields is attractive to simplify qubit manipulation and couple qubits over long distances. Electron spins in silicon offer long lifetimes, but their weak spin-orbit interaction makes electrical coupling challenging. Hole spins bound to acceptor dopants, spin-orbit-coupled  $J = 3/2$  systems similar to Si vacancies in SiC and single Co dopants, are an electrically active spin system in silicon. However,  $J = 3/2$  systems are much less studied than  $S = 1/2$  electrons, and spin readout has not yet been demonstrated for acceptors in silicon. Here, we study acceptor hole spin dynamics by dispersive readout of single-hole tunneling between two coupled acceptors in a nanowire transistor. We identify  $m_J = \pm 1/2$  and  $m_J = \pm 3/2$  levels, and we use a magnetic field to overcome the initial heavy-light hole splitting and to tune the  $J = 3/2$  energy spectrum. We find regimes of spin-like ( $+3/2$  to  $-3/2$ ) and charge-like ( $\pm 1/2$  to  $\pm 3/2$ ) relaxations, separated by a regime of enhanced relaxation induced by mixing of light and heavy holes. The demonstrated control over the energy level ordering and hybridization are new tools in the  $J = 3/2$  system that are crucial to optimize single-atom spin lifetime and electrical coupling.

## INTRODUCTION

Spins in silicon are promising qubits for future quantum information technologies with long spin coherence times in  $^{28}\text{Si}$  and the technological benefit of industry-compatible silicon fabrication processes. Great progress has been made on individual Si:P donor spin qubits including high-fidelity single-qubit logic gates and single-spin measurement (1, 2). Prospects for building large quantum information systems in silicon could be greatly improved by coupling spin qubits to electric fields (3–5) to achieve rapid qubit manipulation and qubit coupling over large distances. However, electron spins in silicon experience weak intrinsic spin-orbit coupling, such that coupling these spin-based qubits to electric fields has, to date, required hybridizing the spin states with valley or charge eigenstates or the use of micrometer-scale magnets (6, 7). These approaches increase the fabrication complexity and introduce extra decoherence channels. Hole spins in the valence band of silicon are an attractive alternative because they have a large intrinsic spin-orbit coupling, and electrical hole spin manipulation has recently been demonstrated in silicon (8).

The development of a single-atom qubit platform that leverages silicon's long spin lifetimes in combination with electrical spin manipulation and long-distance coupling would be highly attractive. Single-acceptor dopant atoms offer strong spin-orbit coupling, making them interesting candidates for electrical manipulation (9–15). Unlike quantum dots, they offer identical confinement potentials, and similar to Si vacancies in SiC and single Co impurities (16–19), they offer the richness of a  $J = 3/2$  manifold to engineer their properties (9–12). For example, it has been recently theoretically predicted that the features of these  $J = 3/2$  manifolds in acceptors allow for electrically mediated long-distance coupling, together with long hole spin lifetimes (11, 12), in addition to earlier predictions on phonon-mediated coupling (9). Yet to date, the properties of  $J = 3/2$  systems are much less studied than their  $S = 1/2$  counterparts. Hole quantum dots in silicon are not expected to have the same qubit engineering possibilities as the single-acceptor qu-

bits due to the strongly broken degeneracy of the  $J = 3/2$  manifold arising from the anisotropic confinement potential of the quantum dots. Moreover, their properties vary considerably from one report to another (8, 20, 21). To date, electrical readout of  $J = 3/2$  systems has not been demonstrated, and the properties of acceptor-bound hole spins have received little attention in the context of quantum information applications.

Here, we demonstrate hole spin readout by detecting spin-dependent tunneling of a single hole between two coupled acceptor dopant atoms in a nanowire transistor fabricated using an industrial process. A dispersive coupling of the two-atom system to a resonator connected to the gate of the transistor realizes the spin readout, which allows us to probe spin relaxation in the closed two-atom system as a function of magnetic field (Zeeman energy  $\epsilon_Z$ ). We also perform single-hole magnetotransport spectroscopy of the two-atom system and identify  $|m_J| = 1/2$  (light hole) and  $|m_J| = 3/2$  (heavy hole) levels within the  $J = 3/2$  manifold and the characteristic splitting  $\Delta_{\text{LH}}$  between them. Combining the singlet-triplet spin relaxation and magnetotransport spectroscopy, we identify regimes  $\epsilon_Z/\Delta_{\text{LH}} < 1$  and  $\epsilon_Z/\Delta_{\text{LH}} > 1$ , where the two-atom dynamics is dominated by relaxation of spin-like ( $3/2$  to  $-3/2$ ) and charge-like ( $3/2$  to  $1/2$ ) degrees of freedom, respectively. These two regimes are separated by a broad relaxation hotspot region of enhanced relaxation induced by hybridization of the  $|m_J| = 3/2$  and  $|m_J| = 1/2$  degrees of freedom. In particular, the demonstrated control over the interplay between magnetic ( $\epsilon_Z$ ) and electric splitting ( $\Delta_{\text{LH}}$ ), together with the hybridization of  $3/2$  and  $1/2$  levels, are the capabilities necessary to optimize spin relaxation, decoherence, and qubit coupling to electric fields. In this way, the benefits of single-atom qubits, such as reproducibly long lifetimes, could potentially be combined with electrically mediated long-distance qubit coupling.

## RESULTS

## Identification of individual acceptors

We use radio frequency (RF) gate reflectometry (22, 23) to detect the charging of localized states in the nanowire transistor, which has previously been used to detect single electrons bound to donors in Si (24),

Copyright © 2018  
The Authors, some  
rights reserved;  
exclusive licensee  
American Association  
for the Advancement  
of Science. No claim to  
original U.S. Government  
Works. Distributed  
under a Creative  
Commons Attribution  
License 4.0 (CC BY).

<sup>1</sup>School of Physics and Australian Centre of Excellence for Quantum Computation and Communication Technology, UNSW, Sydney, Australia. <sup>2</sup>University of Grenoble Alpes and CEA, LETI, MINATEC, 38000 Grenoble, France.

\*Corresponding author. Email: s.rogge@unsw.edu.au

as well as their intersite transitions (25). This charging translates to a shift of the phase,  $\Delta\phi_{\text{refl}}$  or amplitude,  $\Delta A_{\text{refl}}$  of an RF excitation reflected from an LC circuit connected to the top gate, when driven near the resonance frequency with  $V_{\text{RF}}$ . These shifts are a result of the change in admittance of the LC circuit, induced by spin-selective tunneling (26) of holes to and from localized sites. In the measured map of top gate voltage ( $V_{\text{TG}}$ ) and back gate voltage ( $V_{\text{BG}}$ ) shown in Fig. 1B, charging lines appear below the turn on voltage of the nanowire transistor channel (see fig. S1A) because of tunneling back and forth between a localized site and one of the reservoirs. These lines often only appear in small back gate voltage ranges because of the back gate dependence of both the tunnel rates and of the total capacitance of the sensing gate. The states of neutral and positively charged boron atoms are anticipated to contribute to charge transitions furthest below the turn on voltage, as these states are found within the bandgap of silicon. Series of localized states with identical slopes (gray arrows in Fig. 1B) reflect charging events on the same site, likely to be an unintentional quantum dot at the Si/SiO<sub>2</sub> interface (27), while boron atoms bind no more than two holes (28). Another localized site, comparatively less strongly capacitively coupled to the top gate and unaccompanied by lines of equal slope (black arrow in Fig. 1B), indicates the charging of the first hole onto a single-boron atom. We estimate the location of this atom by comparing the capacitive couplings to all four transistor electrodes (see Materials and Methods) and find a position close to the drain lead, inconsistent with a gate-defined quantum dot below the top gate.

A sudden shift in the charging line of this acceptor, shown in Fig. 2A, is the signature of Coulombic interactions with a nearby localized site upon a change in its charge occupation. As we will subsequently argue, the directly probed excited state spectrum of this nearby site is inconsistent with a quantum dot and is expected for a boron atom

binding two holes. The negative  $\Delta\phi_{\text{refl}}$  found within the break of the line indicates the tunneling of holes between the two atoms. A detailed study of the reflected signal in the frequency domain shows that the acceptor-lead tunnel rate is comparable to the resonance frequency (583 MHz) of the LC circuit. In contrast, we find the interacceptor tunnel rate to be much faster than this resonance frequency. We do not observe the tunneling of holes from either lead to the second acceptor atom, likely because of tunnel rates much slower than the resonance frequency. For a complete analysis of all the involved tunnel rates, see section S1 and figs. S1B and S2.

### Dispersively detected Pauli spin blockade in the two-hole system

The magnetic field dependence of the interacceptor signal, shown in Fig. 2B, provides information on the charge occupation of the two-acceptor system. We observe the signature of Pauli spin blockade via the suppression of intersite tunneling with increasing magnetic field (29, 30). This occurs because spins in the triplet state, of which the population increases because of its lowering in energy in the applied magnetic field, cannot tunnel to a singlet state because of the Pauli exclusion principle (see Materials and Methods). This observation of spin-selective tunneling shows that there is an even number of holes bound to the two acceptor atoms. Since acceptors can bind up to two holes (28), we conclude that the observed interacceptor tunneling is a  $(1,1) \leftrightarrow (2,0)$  transition.

The two-hole states of the interacting acceptors (see figs. S4 and S5) reflect the low-energy  $J = 3/2$  manifold that includes both  $\pm 3/2$  and  $\pm 1/2$  states, separated by 20 meV from any additional excited states. In the absence of magnetic fields, an electric potential can split the fourfold degeneracy into two doublets (14, 31, 32), while the presence of magnetic fields will split these doublets via the Zeeman interaction. Figure 2D shows the total energy of the two-hole system at zero magnetic field as a function of the energy level detuning  $\epsilon$  between the atoms, assuming heavy-hole ground states that are consistent with our experiments. To interpret our measurements, it is sufficient to only consider the lowest spin manifold for the  $(1,1)$  configuration (right side of Fig. 2D), where one heavy hole resides on each acceptor, forming a singlet state,  $S_{\text{HH}}$ , and three triplet states,  $T_{\text{HH}}^-$ ,  $T_{\text{HH}}^0$ , and  $T_{\text{HH}}^+$ . For the  $(2,0)$  configuration (left side of Fig. 2D), the doubly occupied acceptor  $A^+$  state, the exchange energy between holes with the same angular momentum ( $J_{\text{HH}}$  and  $J_{\text{LL}}$ ) or different angular momenta ( $J_{\text{LH}} = J_{\text{HL}}$ ) obey  $J_{\text{HH}}, J_{\text{LL}} > J_{\text{LH}} > J_{\text{LH}}$  in our experiments. In analogy to the two-hole states of neutral group II acceptors (33) and of two closely spaced boron atoms (15), the lowest energy manifold in the  $(2,0)$  configuration consists of six states, split by  $\Delta_{\text{LH}}$  and  $J_{\text{LH}}$ . The ground state is the heavy hole singlet,  $S_{\text{HH}}$ . Four states consisting of one heavy hole and one light hole,  $Q_{\text{LH}}^i$ , with  $i$  denoting the angular momentum, are approximately  $\Delta_{\text{LH}}$  higher in energy and split by  $J_{\text{LH}}$  into singlet and triplet states, as shown in Fig. 2D. The sixth state is the light hole singlet state,  $S_{\text{LL}}$ , approximately another  $\Delta_{\text{LH}}$  higher in energy. For most of the presented analysis, it is sufficient to only consider the  $S_{\text{HH}}$ ,  $T_{\text{HH}}^-$ , and  $Q_{\text{LH}}^{2-}$  states, which, for simplicity, we will from now on refer to as the  $S$ ,  $T$ , and  $Q$  states.

At zero magnetic field, the tunnel coupling  $t$  between the  $(1,1)$   $S$  and  $(2,0)$   $S$  states gives rise to the interacceptor reflectometry signal, with  $t$  measured by a microwave excitation experiment to be  $4.3 \pm 0.3$  GHz (see section S1 and fig. S3) (34). At a finite magnetic field, which we label  $B_{S \rightarrow T}$ , the  $(1,1)$   $T$  state becomes the ground state at the zero detuning point. Using the tunnel coupling  $t$  and the thermal

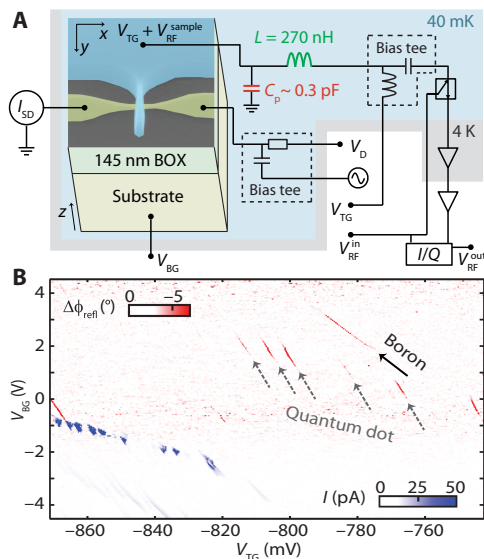


**Fig. 1. Detection of a single acceptor atom.** (A) Scanning electron microscopy image of the used tri-gate transistor in a schematic diagram of the experimental setup for transport and RF gate reflectometry measurements. The magnetic field in this experiment is applied along the  $y$  direction (along the channel). (B) Change in reflected phase from the LC circuit (red) compared to the measured source-drain current (blue), both at 1 mV  $V_D$ . The signals of a boron atom (black arrow) and an unintentional quantum dot (gray arrows) are identified. BOX, buried oxide.

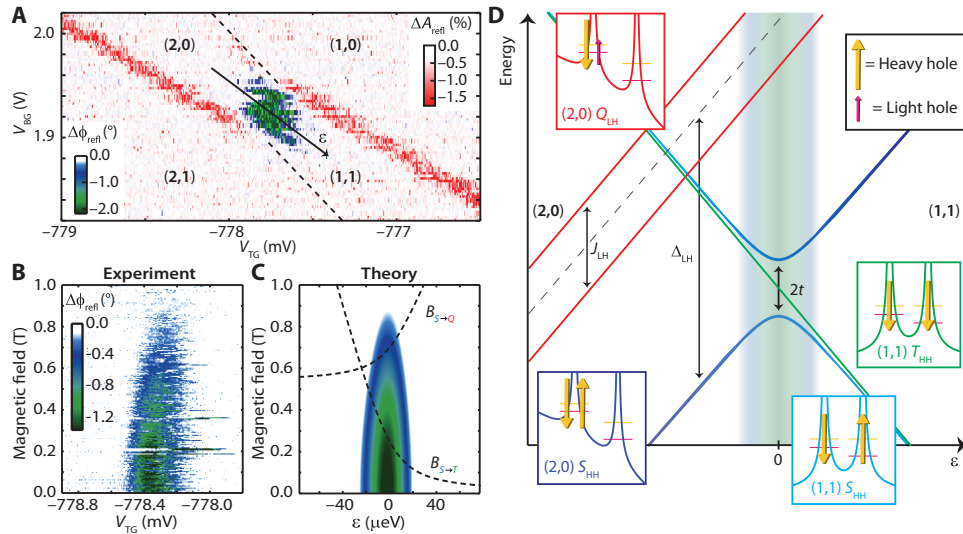


**Fig. 2. Two-hole system.** (A) Reflected amplitude and phase response showing a break in the acceptor-lead charging line (red) caused by the charging of a nearby acceptor atom (dashed lines). (B and C) Measured and calculated magnetic field dependence of the interacceptor tunneling phase response. The magnetic fields yielding the singlet-triplet crossing  $B_{S \rightarrow T}$  and singlet-quadruplet crossing  $B_{S \rightarrow Q}$  are plotted in (C) as a function of detuning by dashed curves. (D) Schematic overview of the relevant two-hole states. The (1,1) and (2,0)  $S_{\text{HH}}$  states (blue), (1,1)  $T_{\text{HH}}$  states (green), and (2,0)  $Q_{\text{LH}}$  states (red) are shown. While this subset of two-hole states is sufficient to describe our experiments, a full description of the spin-orbit states can be found in section S3. Insets show a depiction of the potential landscape and possible spins involved in these states.

occupation of the two-hole states (see Materials and Methods), we simulate this magnetic field dependence of the reflectometry signal (35), as shown in Fig. 2C. From the simulation, we estimate  $B_{S \rightarrow T}$  at  $0.25 \pm 0.05$  T, which provides an effective Landé  $g$  factor ( $g^* = gm_f$ ) of the  $T$  state of  $1.2 \pm 0.3$ , using the Zeeman energy of  $g^* \mu_B B$ , where  $\mu_B$  is the Bohr magneton. In this low-magnetic field regime, we find that  $g^*$  is suppressed compared to an acceptor state with cubic site symmetry, for which  $\Delta m_f = 3$  and  $g \approx 1$  ( $g^* \approx 3$ ) are expected. For an acceptor atom, this suppression of  $g^*$  can occur when the magnetic field splitting is smaller than the heavy-light hole splitting set by an electric potential that could originate from local strain, an electric field, or a nearby interface (fig. S4B).

### Relaxation and hybridization of $\pm 3/2$ and $\pm 1/2$ states

We investigated spin relaxation of the two-hole system by time-dependent gate reflectometry using pulsed gate voltages. Specifically, we generate a nonequilibrium singlet population by pulsing the system via the (2,1) region into the (2,0) state and monitoring the inter-site tunneling at the (1,1)  $\leftrightarrow$  (2,0) degeneracy point. The asymmetry in tunnel rates to both acceptors (see section S1) ensures that the charge transition via the (2,0) state is much more likely than the direct transition from the (2,1) state to the (1,1) state in this pulse scheme. The nonequilibrium singlet tunneling signal, indicated by the white circle in Fig. 3A, is obtained by pulsing 0.8 mV on the drain electrode to the readout point  $\epsilon_0$  for 160 ns, after spending 40 ns at  $\epsilon_1$ , in a magnetic field of 1.5 T. The transient decay of this phase response shown in Fig. 3B reflects the singlet probability decay by relaxation at the degeneracy point (36), averaged over  $10^6$  sequences, for the modified pulse timing shown in the inset of Fig. 3B and the same detunings  $\epsilon_0$  and  $\epsilon_1$  as in Fig. 3A.

By fitting the measured singlet decay for different magnetic fields, we obtain the relaxation rates in Fig. 3C. Above 1.5 T,  $T_1^{-1}$  increases with magnetic field in agreement with spin-lattice relaxation (9, 37),

but below 1.5 T,  $T_1^{-1}$  reaches a maximum around  $\sim 0.8$  T, which is not expected for spin-lattice relaxation. We also rule out nuclear spin-induced hole spin relaxation as this would occur at smaller magnetic fields. Rather, these measurements resemble the relaxation observed at degeneracy points for spin and orbital degrees of freedom (38, 39). A schematic of the magnetic field dependence of two-hole states (Fig. 3D) identifies degeneracy points  $B_{S \rightarrow T}$ , where the (1,1)  $T$  state falls below the singlet, and  $B_{S \rightarrow Q}$ , where the (2,0)  $Q$  state falls below the singlet. We fit the data in Fig. 3C to a model that takes into account various relaxation mechanisms. These include the spin-lattice relaxation  $\Gamma_{S \rightarrow T}$  from the  $S$  state to the  $T$  state, which requires a heavy hole spin flip ( $\Delta m_f = 3$  relaxation), and the relaxation  $\Gamma_{S \rightarrow Q}$  from the  $S$  state to the  $Q$  state, which requires a flip from a light hole to a heavy hole ( $\Delta m_f = 2$  relaxation). Both of these spin-lattice relaxation rates have a monotonic power law dependence on magnetic field, as described by

$$\Gamma_{S \rightarrow T[Q]} = A_{ST[Q]} \left( (B - B_{S \rightarrow T[Q]})^2 + (2t_{ST[Q]})^2 \right)^{\gamma_{ST[Q]}/2} \quad (1)$$

with  $A_{ST[Q]}$  being the relaxation amplitude for the  $S \rightarrow T[Q]$  process and  $t_{ST[Q]}$  being the coupling of the  $S$  state and the (1,1)  $T$  [(2,0)  $Q$ ] state. A  $\gamma_{SQ}$  of 3 characterizes the  $\Delta m_f = 2$  (light to heavy hole) relaxation because it has a strong charge-like character and is therefore directly allowed by phonons. The  $\Delta m_f = 3$  relaxation is characterized by  $\gamma_{ST} = 5$  and should be weaker than the  $\Delta m_f = 2$  transition, since it involves a less direct heavy hole spin flip (9, 11).

A light-heavy hole tunneling-induced hybridization between the  $S$  and  $Q$  states causes the anticrossing at  $B_{S \rightarrow Q}$  (Fig. 3D). Here, we expect a spin relaxation hotspot (38, 40, 41), since the finite light hole component opens a light-to-heavy hole relaxation path to the (1,1)  $T$  state with relaxation rate  $\Gamma_{S/Q \rightarrow T}$ , which is expected to be much faster than the heavy-to-heavy hole relaxation process  $\Gamma_{S \rightarrow T}$  (9, 11).

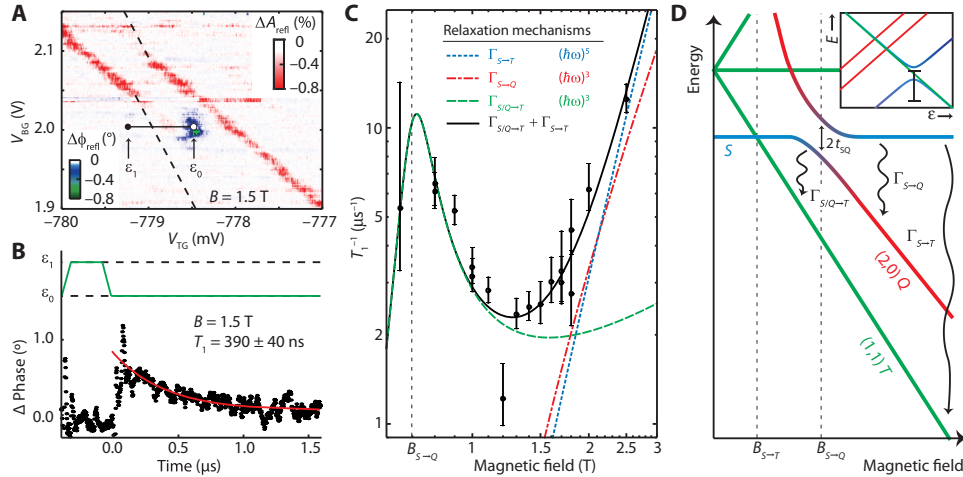


**Fig. 3. Spin relaxation mechanisms of the two-hole system.** (A) Time-averaged RF reflectometry amplitude (red) and phase (blue) measurement with continuous pulses applied to the drain, at a magnetic field of 1.5 T. The interacceptor tunneling is displaced from the break of the acceptor-lead tunneling signal by the Zeeman energy of the T ground state. (B) Relaxation time extracted from the time-dependent phase signal for a pulse between the points  $\epsilon_0$  and  $\epsilon_1$ . (C) Magnetic field dependence of the relaxation rate  $T_1^{-1}$ . (D) Schematic view of the relevant relaxation rates in this system at the zero detuning point (see inset). The data in (C) are fit to a combination of the  $\Gamma_{S/Q \rightarrow T}$  rate (green line) and  $\Gamma_{S \rightarrow T}$  rate (blue line), resulting in the black line. This is compared to a fit using the  $\Gamma_{S \rightarrow Q}$  rate (red line) instead of the  $\Gamma_{S \rightarrow T}$  rate.

This relaxation strongly depends on the light hole component in the hybridized states (see Materials and Methods), and we obtain

$$\Gamma_{S/Q \rightarrow T} = A_{QT} \frac{2t_{SQ}^2(B - B_{S \rightarrow T})^3}{(B - B_{S \rightarrow Q})^2 + (2t_{SQ})^2} \quad (2)$$

with  $A_{QT}$  being the relaxation amplitude between the Q and T states.

The sum of  $\Gamma_{S \rightarrow T}$  and  $\Gamma_{S/Q \rightarrow T}$  gives a satisfactory least squares fit to the magnetic field dependence of  $T_1^{-1}$ , as shown by a solid black line in Fig. 3C. Our fit yields  $B_{S \rightarrow Q} = 0.70 \pm 0.02$  T at the anticrossing point and an asymmetry  $A_{QT}/A_{ST} \approx 1.2 \times 10^3$ , although we could not determine the exponent of the spin relaxation mechanism above 1.5 T, as shown in fig. S6 (see also section S4). The large asymmetry  $A_{QT}/A_{ST}$  reflects the faster  $\Delta m_j = 2$  relaxation (light to heavy hole) compared to  $\Delta m_j = 3$  relaxation (heavy hole up to heavy hole down), as expected because the  $\Delta m_j = 2$  relaxation is mediated directly by phonons.

The spectral width of the hotspot in Fig. 3C reflects the direct tunnel coupling-induced hybridization between the Q state, which contains one heavy hole and one light hole, and the S state of two heavy holes. Our fit of the  $T_1$  lineshape yields a tunnel coupling  $t_{SQ} = 0.04 \pm 0.015$  T, which converts to an energy between 3.5  $\mu$ eV (840 MHz) and 7  $\mu$ eV (1.6 GHz), assuming  $g^*$  between 1.5 and 3.0. Since the singlet is actually a superposition of (2,0) and (1,1) charge configurations,  $t_{SQ}$  includes contributions involving tunneling to the other atom [for the (1,1) singlet] and no tunneling to the other atom [for the (2,0) singlet]. Given that the intersite tunnel coupling of the heavy holes is 4.3 GHz (fig. S3), and heavy-to-light hole intersite tunneling is expected to be a factor of  $\sim 10$  weaker ( $\sim 430$  MHz) (15), we expect that the bulk of the tunneling between the light and heavy holes is an on-site hybridization that occurs on the same atom.

This on-site hybridization of  $|m_j| = 1/2$  and  $3/2$  states is a key property of quantum bits in  $J = 3/2$  systems. Increasing the degree of hybridization can be used to increase the splitting  $\Delta$  to enhance qubit relaxation times (9–12) or to mix the  $|m_j| = 1/2$  with the  $|m_j| = 3/2$  states to obtain fast electric drive, together with charge-noise in-

sensitivity at sweet spots (10, 11). Assuming that the mixing is caused by the lowest-order electric field coupling, we find an electric field component  $E = t_{SQ}/p \sim 0.17$  MV/m to 0.34 MV/m causing the anti-crossing at the degeneracy point, where  $p \approx 0.26$  D is the  $T_d$  symmetry light-to-heavy hole dipole coupling (42, 43). For large gate electric fields (20 MV/m), which can be tolerated near interfaces, these couplings extrapolate to  $\sim 100$  GHz light-to-heavy hole mixings. As required to realize the theoretically predicted sweet spots (10, 11), the mixing at the high gate field exceeds typical qubit Larmor frequencies. Notably, the larger gate fields are also required to obtain a very strong coupling of the qubit state to electric fields via a Rashba-like interaction (10, 11).

### Tuning the two-hole spectrum

To further understand the coupled acceptor system, we perform excited state spectroscopy by single-hole tunneling transport (13, 20, 21). In Fig. 4A, the transconductance signal as a function of  $V_{TG}$  and  $V_{BG}$  at zero magnetic field shows a bias triangle (contour marked by a solid line), demonstrating sequential hole tunneling via both acceptors in series. We attribute lines parallel to the triangle baseline (arrows in Fig. 4A) to transitions from the (1,1) ground state to the (2,0) excited states (see section S5 and figs. S4 and S5). The observed (2,0) spectrum matches the expected energy spectrum of a doubly charged acceptor state, as shown in Fig. 4B. This supports our identification of the second confinement site as an acceptor atom, further validated by the incompatibility of our measurement with the regularly spaced excited state spectrum expected for quantum dots. The (2,0)  $\Delta_{LH}$  and  $J_{LH}$  are extracted as  $110 \pm 10$   $\mu$ eV and  $36 \pm 5$   $\mu$ eV, respectively. The exchange splitting  $J_{LH}$  is not to be confused with the tunnel coupling between light and heavy hole states at the magnetic field-induced degeneracy. Rather, it describes the energy lowering of two-hole states on a single atom due to hybridization induced by Coulomb interactions (33). Nevertheless,  $J_{LH}$  reflects a tunneling process between light and heavy holes, so it is not unexpected that it is of the order of  $t_{SQ}$ .

The splitting  $\Delta_{LH}$  between the  $m_j = 3/2$  and  $m_j = 1/2$  states at zero magnetic field is a key parameter for qubits in  $J = 3/2$  systems, since

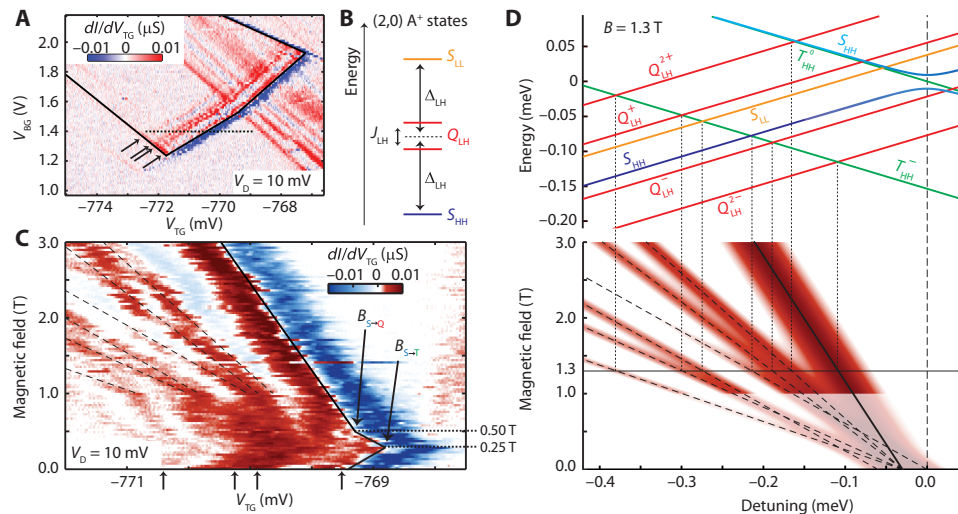


**Fig. 4. Excited states of the two-hole system measured by transport spectroscopy.** (A) Transconductance  $dI/dV_{TG}$  as a function of the top and back gate voltages at 10 mV  $V_D$ . The bias triangle, marked by solid black lines, shows three excited states in addition to the ground state as indicated by arrows. (B) Level configuration of the  $A^+$  state, corresponding to the found excited states. (C) Magnetic field dependence of the transconductance at a cut through the bias triangle at 1.4 V  $V_{BG}$ , as indicated by the dotted line in (A). At the bottom, arrows indicate the excited state spectrum as also shown in (A). Two changes in the slope of the ground state at 0.25 and 0.5 T are the result of the  $B_{S \rightarrow T}$  and  $B_{S \rightarrow Q}$  crossings. (D) Model of the transition energies in the high-magnetic field limit. Top: Overview of the  $(1,1) \rightarrow (2,0)$  transitions at a magnetic field of 1.3 T. Bottom: Simulated magnetic field behavior of the transition energy spectrum, using the  $g$  factors and  $\Delta_{LH}$  extracted from the transition energies in (C) and using the same line broadening as found in this experiment.

its interplay with the Zeeman interaction  $\epsilon_Z$  determines the qubit properties (9, 42). The two-level system formed by the lowest-energy states is charge-like when  $\epsilon_Z > |\Delta_{LH}|$  and spin-like when  $\epsilon_Z < |\Delta_{LH}|$ . For an acceptor in silicon, a nonzero  $\Delta_{LH}$  can only reflect a lowered symmetry of the acceptor state due to an electric potential that lacks the cubic symmetry of the silicon lattice (31, 42). The perturbation of this electric potential causes mixing and splitting of the  $J = 3/2$  states independently of the Zeeman interaction, resulting in a host of distinct properties (43) that are absent for conventional  $S = 1/2$  electron spins. Especially, when this perturbation dominates the Zeeman interaction ( $\epsilon_Z < \Delta_{LH}$ ) and is applied along a different direction from the magnetic field, it results in a reduced  $g^*$  (43).

To investigate the crossover from  $\epsilon_Z < |\Delta_{LH}|$  to  $\epsilon_Z > |\Delta_{LH}|$ , we compare the transition energy spectrum including high magnetic field data with the spin blockade data at low magnetic fields. We measured the excited state data as a function of magnetic field, as shown in Fig. 4C, on a cut through the bias triangle at  $V_{BG} = 1.4$  V (dotted line in Fig. 4A). The baseline of the triangle, indicated with a solid line in Fig. 4C, changes its slope twice. The first change around 0.25 T indicates the singlet-triplet crossing at  $B_{S \rightarrow T}$ , in agreement with the observation of spin blockade in Fig. 2B. The second change around 0.50 T indicates the change of the  $(2,0)$  ground state from  $S$  to  $Q$ , corresponding to the same anticrossing that generates the relaxation hotspot in Fig. 3B but here occurring in the negative detuning region and therefore at a lower magnetic field.

In the high-magnetic field regime ( $>1$  T), we observe clear resonance lines outnumbering those at zero magnetic field, indicating spin-split excited states. In this regime, the Zeeman energy dominates over  $\Delta_{LH}$ , and therefore, the angular momenta of the two-hole states align with the external magnetic field. Ignoring any mixing terms other than the mixing of the  $S$  state, the magnetic field dependence of the transition energies can be easily described by using  $m_j = \pm 3/2$  for heavy holes and  $m_j = \pm 1/2$  for light holes to calculate the Zeeman shifts, as shown in Fig. 4D. Using this model, we extract the  $g$  factors and  $\Delta_{LH}$

by fitting the slopes and position of the transition lines in Fig. 4C, respectively. For the doubly occupied acceptor, we find  $g_{3/2}$  of 0.85 and  $g_{1/2}$  of 1.07 and  $\Delta_{LH}$  of 30  $\mu$ eV. For the singly occupied acceptor, only the heavy hole states play a role in the transitions for which we extract  $g_{3/2}$  of 1.05. Note that, here, we use  $m_j$  to determine the  $g$  factor instead of the effective  $g$  factor  $g^*$ .

A comparison of the low-magnetic field (spin blockade) and high-magnetic field (transport spectroscopy) measurements demonstrates the changes in the  $J = 3/2$  system between the  $\epsilon_Z < |\Delta_{LH}|$  and  $\epsilon_Z > |\Delta_{LH}|$  regimes. The  $g$  factors found in the high-magnetic field regime are close to those found for bulk boron acceptors (44, 45), contrasting the smaller effective  $g$  factor found at low magnetic fields in the spin blockade experiment in Fig. 2B, when the acceptor system is dominated by the perturbation of an electric potential. Furthermore, the  $\Delta_{LH}$  of the doubly occupied acceptor is about four times smaller in the high-magnetic field regime than at zero magnetic field. A further indication of the crossover between different regimes of the  $J = 3/2$  system is the appearance of transport signal attributed to the  $(1,1) T$  to  $(2,0) S$  transition when  $\epsilon_Z < |\Delta_{LH}|$ . This transition is prohibited by the Pauli principle when the total angular momenta are aligned with the external magnetic field, resulting in the absence of a corresponding transport feature at magnetic fields higher than 2 T. At small magnetic fields, on the other hand, the mixing of the  $J = 3/2$  states allows this transition, and thus, the corresponding transport feature appears. The crossover between  $\epsilon_Z < |\Delta_{LH}|$  and  $\epsilon_Z > |\Delta_{LH}|$  reflects a controlled transition between the regimes dictated by spin physics and charge physics, which is a unique feature of the  $J = 3/2$  systems.

## DISCUSSION

We have demonstrated the readout of the spin state of two coupled atoms using a reflected RF signal from a resonator connected to the gate of a nanowire transistor and the Pauli exclusion principle (46). Given that the readout scheme requires a tank circuit on the gate

electrode and avoids the use of a single-electron transistor, it could be exploited to simplify the readout in a scalable quantum computing architecture. Using this spin readout scheme, we have investigated the lifetime of spin excitations at the charge degeneracy point of the two atoms and found a magnetic field–induced anticrossing caused by hybridization between  $|m_j| = 3/2$  and  $|m_j| = 1/2$  spin degrees of freedom. Combined with transport spectroscopy data, we also found that it is possible to tune between regimes defined by the heavy-light hole splitting and defined by the Zeeman energy. This allows the change between a spin physics– and a charge physics–dominated system, thereby controlling the  $g$  factor and heavy-light hole splitting of the  $J = 3/2$  system, which has no analog in a  $S = 1/2$  system. In the future, larger splittings  $\Delta_{\text{LH}}$  induced by confinement or strain can be used to enhance qubit lifetime, and higher gate electric fields can be used to enhance qubit coupling to electric fields.

## MATERIALS AND METHODS

### Experimental design

The silicon nanowire transistor used in this work was fabricated using a standard complementary metal-oxide semiconductor technology, similar to previously reported devices (21, 24). The channel, defined by the top gate, is 11 nm high, 42 nm wide, and 54 nm long. On both sides of this gate, 25-nm-long  $\text{Si}_3\text{N}_4$  spacers form barriers to the highly doped source and drain regions. With a background boron doping of  $5 \times 10^{17} \text{ cm}^{-3}$  in the silicon channel, about 10 boron atoms are expected under the gate and about 10 are expected under the spacers.

In a dilution refrigerator at a base temperature of 40 mK, hole transport and RF gate reflectometry measurements give complementary insights into the static and dynamic behavior of the two-hole system of interest. The hole temperature was measured from quantum dot transport at  $\sim 300$  mK. The noise floor of the transport measurement ( $\sim 100$  fA) allows us to detect currents with a total tunnel rate down to 500 kHz. A surface mount 270-nH inductor, attached to the top gate, forms a tank circuit together with a parasitic capacitance of  $\sim 0.3$  pF. Tunnel events in the transistor with a tunnel rate higher than or equal to the resonance frequency of 583 MHz result in a change of the reflected amplitude and/or phase of this resonator. Furthermore, low-intensity light was directed to the silicon chip through an optical fiber to enable the use of the lower doped substrate as a back gate.

### Location of the acceptors

To estimate the location of the two atoms, we extracted the relative capacitive coupling to the different electrodes. The hole temperature of  $\sim 300$  mK gives  $k_B T \gg \hbar \Gamma$  for the acceptor-lead tunnel rate, thereby justifying a thermally broadened fit (25). The reflectometry linewidth shows a relative coupling to the top gate ( $\alpha_{\text{TG}}$ ) and drain ( $\alpha_{\text{D}}$ ) of  $0.50 \pm 0.01$  eV/V and  $0.41 \pm 0.02$  eV/V, respectively, thereby placing this atom roughly halfway between these two electrodes, under the  $\text{Si}_3\text{N}_4$  spacer. This relatively weak coupling to the top gate supports our identification of the acceptor atom, as gate-induced quantum dots are known to have gate couplings above  $\sim 0.7$  eV/V (24, 27). The second boron atom has to be located closer to the center of the channel, as the tunneling to both electrodes is too slow to be detected.

### Pauli spin blockade in RF gate reflectometry

The shift in phase response of the reflected signal, as shown in Fig. 2B, is ascribed to the addition of a quantum capacitance ( $C_Q$ ) to the

LC circuit (22–25) when holes can tunnel between the two atoms, given by

$$C_Q = \frac{1}{2} \Delta \alpha_{\text{TG}}^2 q^2 4t^2 (\epsilon^2 + 2t^2)^{-3/2} \quad (3)$$

where  $\Delta \alpha_{\text{TG}}$  is the difference in capacitive coupling from the top gate to each acceptor (found to be 0.14 eV/V in the transport measurements),  $q$  is the electron charge,  $\epsilon$  is the energy detuning between the two acceptors, and  $t$  is the tunnel coupling between the (1,1) and (2,0) S states. All other tunnel couplings between the (1,1) and (2,0) states are considered to be much smaller and therefore not contributing to a change in the detected reflected signal. The total phase shift ( $\Delta \phi$ ) was determined by the difference in occupation, given by the Boltzmann distribution, of the lower and upper branches of the heavy hole singlet state (35)

$$\Delta \phi \sim C_Q \frac{e^{(-E_{S-}/kT)} - e^{(-E_{S+}/kT)}}{\sum e^{(-E_i/kT)}} \quad (4)$$

where  $E_{S-}$  and  $E_{S+}$  are the energies of the bonding and antibonding singlet states, respectively, and  $E_i$  describes the energies of all the involved states. Using Eqs. 3 and 4, the magnetic field dependence of the phase shift caused by the interacceptor tunneling was calculated, as shown in Fig. 2C. We note that, although the crossing of the Q state and the S state has some influence on the Boltzmann distribution of the S states, this influence is not distinguishable in the measurement. However, for completeness, we displayed the  $B_{S \rightarrow Q}$  crossing point in Fig. 2C, as found in the relaxation hotspot measurement, together with an estimated  $g$  factor of the Q state.

### Relaxation hotspot

The observed relaxation hotspot is explained by the mixing of the bonding S state and the (2,0) Q state, which allows a light-to-heavy hole relaxation to the (1,1) T state. This relaxation process is expected to have a  $(\hbar \omega)^3$  dependence and furthermore depends linearly on the light hole character of the mixed state. Here, we show the calculation of the light hole character of the probed state. Around the anticrossing, we can write the energies of the lower (–) and upper (+) states as

$$E_{\pm} = \frac{\Delta E}{2} \pm \frac{1}{2} \sqrt{(\Delta E)^2 + (2t_{\text{SQ}})^2} \quad (5)$$

where  $\Delta E$  is the energy splitting between the states in the absence of mixing ( $E_Q - E_S$ ), and  $E_S$  is taken as the reference energy ( $E = 0$ ). We defined the amount of light hole character of each state as the chance to measure it as the Q state in the basis of Q and S, written as  $\xi_{\pm}$  and given by

$$\xi_{\pm} = \frac{1}{2} \frac{\Delta E}{\sqrt{(\Delta E)^2 + (2t_{\text{SQ}})^2}} \quad (6)$$

The relaxation measurement was performed at zero detuning, which is the original position of  $E_S$  in the absence of mixing. The state probed here can be written as a combination of the positive (+) and negative (–) states, depending on their relative energy difference with the measurement point  $|E_{\pm}|/(|E_{-}| + |E_{+}|)$ . We note that  $|E_{-}|\xi_{-} = |E_{+}|\xi_{+} = t_{\text{SQ}}^2 / \sqrt{(\Delta E)^2 + (2t_{\text{SQ}})^2}$  and also that  $(|E_{-}| + |E_{+}|)$  is equal

to  $\sqrt{(\Delta E)^2 + (2t_{\text{SQ}})^2}$ , which gives the total light hole character at the zero energy point as

$$\xi_{E=0} = \frac{|E_-|\xi_- + |E_+|\xi_+}{|E_-| + |E_+|} = \frac{2t_{\text{SQ}}^2}{(\Delta E)^2 + (2t_{\text{SQ}})^2} \quad (7)$$

as used in Eq. 2.

## SUPPLEMENTARY MATERIALS

Supplementary material for this article is available at <http://advances.sciencemag.org/cgi/content/full/4/12/eaat9199/DC1>

Section S1. Estimation of tunnel rates

Section S2. Acceptor-based single-atom qubits

Section S3. Two-hole states

Section S4. Relaxation mechanisms

Section S5.  $(1,1) \rightarrow (2,0)$  transition energies

Fig. S1. Transport spectroscopy images.

Fig. S2. Frequency domain analysis of the reflectometry signal.

Fig. S3. Interacceptor continuous-wave microwave excitation experiment.

Fig. S4. Examples of the Zeeman effect on  $A^0$  states.

Fig. S5. Examples of the Zeeman effect on two-hole states.

Fig. S6. Relaxation rate models.

References (47–51)

## REFERENCES AND NOTES

- J. J. Pla, K. Y. Tan, J. P. Dehollain, W. H. Kim, J. J. L. Morton, D. N. Jamieson, A. S. Dzurak, A. Morello, A single-atom electron spin qubit in silicon. *Nature* **489**, 541–545 (2012).
- J. T. Muhonen, J. P. Dehollain, A. Laucht, F. E. Hudson, R. Kalra, T. Sekiguchi, K. M. Itoh, D. N. Jamieson, J. C. McCallum, A. S. Dzurak, A. Morello, Storing quantum information for 30 seconds in a nanoelectronic device. *Nat. Nanotechnol.* **9**, 986–991 (2014).
- K. C. Nowack, F. H. L. Koppens, Yu. V. Nazarov, L. M. K. Vandersypen, Coherent control of a single electron spin with electric fields. *Science* **318**, 1430–1433 (2007).
- M. Pioro-Ladrière, T. Obata, Y. Tokura, Y.-S. Shin, T. Kubo, K. Yoshida, T. Taniyama, S. Tarucha, Electrically driven single-electron spin resonance in a slanting Zeeman field. *Nat. Phys.* **4**, 776–779 (2008).
- J. Medford, J. Beil, J. M. Taylor, S. D. Bartlett, A. C. Doherty, E. I. Rashba, D. P. DiVincenzo, H. Lu, A. C. Gossard, C. M. Marcus, Self-consistent measurement and state tomography of an exchange-only spin qubit. *Nat. Nanotechnol.* **8**, 654–659 (2013).
- K. Takeda, J. Kamioka, T. Otsuka, J. Yoneda, T. Nakajima, M. R. Delbecq, S. Amaha, G. Allison, T. Kodera, S. Oda, S. Tarucha, A fault-tolerant addressable spin qubit in a natural silicon quantum dot. *Sci. Adv.* **2**, e1600694 (2016).
- D. Kim, Z. Shi, C. B. Simmons, D. R. Ward, J. R. Prance, T. S. Koh, J. K. Gamble, D. E. Savage, M. G. Lagally, M. Friesen, S. N. Coppersmith, M. A. Eriksson, Quantum control and process tomography of a semiconductor quantum dot hybrid qubit. *Nature* **511**, 70–74 (2014).
- R. Maurand, X. Jehl, D. Kotekar-Patil, A. Corna, H. Bohoslavskiy, R. Laviéville, L. Hutin, S. Barraud, M. Vinet, M. Sanquer, S. De Franceschi, A CMOS silicon spin qubit. *Nat. Commun.* **7**, 13575 (2016).
- R. Ruskov, C. Tahan, On-chip cavity quantum phonodynamics with an acceptor qubit in silicon. *Phys. Rev. B* **88**, 064308 (2013).
- J. Salfi, M. Tong, S. Rogge, D. Culcer, Quantum computing with acceptor spins in silicon. *Nanotechnology* **27**, 244001 (2016).
- J. Salfi, J. A. Mol, D. Culcer, S. Rogge, Charge insensitive single-atom spin-orbit qubit in silicon. *Phys. Rev. Lett.* **116**, 246801 (2016).
- J. C. Abadillo-Uriel, M. J. Calderón, Interface effects on acceptor qubits in silicon and germanium. *Nanotechnology* **27**, 024003 (2016).
- J. van der Heijden, J. Salfi, J. A. Mol, J. Verduijn, G. C. Tettamanzi, A. R. Hamilton, N. Collaert, S. Rogge, Probing the spin states of a single acceptor atom. *Nano Lett.* **14**, 1492–1496 (2014).
- J. A. Mol, J. Salfi, R. Rahman, Y. Hsueh, J. A. Miwa, G. Klimeck, M. Y. Simmons, S. Rogge, Interface-induced heavy-hole/light-hole splitting of acceptors in silicon. *Appl. Phys. Lett.* **106**, 203110 (2015).
- J. Salfi, J. A. Mol, R. Rahman, G. Klimeck, M. Y. Simmons, L. C. L. Hollenberg, S. Rogge, Quantum simulation of the Hubbard model with dopant atoms in silicon. *Nat. Commun.* **7**, 11342 (2016).
- H. Kraus, V. A. Soltamov, D. Riedel, S. Vāth, F. Fuchs, A. Sperlich, P. G. Baranov, V. Dyakonov, G. V. Astakhov, Room-temperature quantum microwave emitters based on spin defects in silicon carbide. *Nat. Phys.* **10**, 157–162 (2014).
- M. Widmann, S.-Y. Lee, T. Rendler, N. T. Son, H. Fedder, S. Paik, L.-P. Yang, N. Zhao, S. Yang, I. Booker, A. Denisenko, M. Jamali, S. A. Momenzadeh, I. Gerhardt, T. Ohshima, A. Gali, E. Janzén, J. Wrachtrup, Coherent control of single spins in silicon carbide at room temperature. *Nat. Mater.* **14**, 164–168 (2015).
- A. F. Otte, M. Ternes, K. von Bergmann, S. Loth, H. Brune, C. P. Lutz, C. F. Hirjibehedin, A. J. Heinrich, The role of magnetic anisotropy in the Kondo effect. *Nat. Phys.* **4**, 847–850 (2008).
- R. Toskovic, R. van den Berg, A. Spinelli, I. S. Eliens, B. van den Toorn, B. Bryant, J.-S. Caux, A. F. Otte, Atomic spin-chain realization of a model for quantum criticality. *Nat. Phys.* **12**, 656–660 (2016).
- R. Li, F. E. Hudson, A. S. Dzurak, A. R. Hamilton, Pauli spin blockade of heavy holes in a silicon double quantum dot. *Nano Lett.* **15**, 7314–7318 (2015).
- B. Voisin, R. Maurand, S. Barraud, M. Vinet, X. Jehl, M. Sanquer, J. Renard, S. De Franceschi, Electrical control of  $g$ -factor in a few hole silicon nanowire MOSFET. *Nano Lett.* **16**, 88–92 (2016).
- K. D. Petersson, C. G. Smith, D. Anderson, P. Atkinson, G. A. C. Jones, D. A. Ritchie, Charge and spin state readout of a double quantum dot coupled to a resonator. *Nano Lett.* **10**, 2789–2793 (2010).
- J. I. Colless, A. C. Mahoney, J. M. Hornibrook, A. C. Doherty, H. Lu, A. C. Gossard, D. J. Reilly, Dispersive readout of a few-electron double quantum dot with fast rf gate sensors. *Phys. Rev. Lett.* **110**, 046805 (2013).
- M. F. Gonzalez-Zalba, S. Barraud, A. J. Ferguson, A. C. Betz, Probing the limits of gate-based charge sensing. *Nat. Commun.* **6**, 6084 (2015).
- M. G. House, T. Kobayashi, B. Weber, S. J. Hille, T. F. Watson, J. van der Heijden, S. Rogge, M. Y. Simmons, Radio frequency measurements of tunnel couplings and singlet-triplet spin states in SiP quantum dots. *Nat. Commun.* **6**, 8848 (2015).
- A. C. Johnson, J. R. Petta, J. M. Taylor, A. Yacoby, M. D. Lukin, C. M. Marcus, M. P. Hanson, A. C. Gossard, Triplet-singlet spin relaxation via nuclei in a double quantum dot. *Nature* **435**, 925–928 (2005).
- B. Voisin, V.-H. Nguyen, J. Renard, X. Jehl, S. Barraud, F. Triozon, M. Vinet, I. Duchein, Y.-M. Niquet, S. De Franceschi, M. Sanquer, Few-electron edge-state quantum dots in a silicon nanowire field-effect transistor. *Nano Lett.* **14**, 2094–2098 (2014).
- V. N. Aleksandrov, E. M. Gershenzon, A. P. Mel'nikov, R. I. Rabinovich, N. A. Serebryakova, Interaction of  $A^+$  ( $D^+$ ) centers in semiconductors with charged and neutral impurities. *JETP Lett.* **22**, 282–283 (1975).
- F. H. L. Koppens, J. A. Folk, J. M. Elzerman, R. Hanson, L. H. Willems van Beveren, I. T. Vink, H. P. Tranitz, W. Wegscheider, L. P. Kouwenhoven, L. M. K. Vandersypen, Control and detection of singlet-triplet mixing in a random nuclear field. *Science* **309**, 1346–1350 (2005).
- J. R. Petta, A. C. Johnson, J. M. Taylor, E. A. Laird, A. Yacoby, M. D. Lukin, C. M. Marcus, M. P. Hanson, A. C. Gossard, Coherent manipulation of coupled electron spins in semiconductor quantum dots. *Science* **309**, 2180–2184 (2005).
- L. E. Calvet, R. G. Wheeler, M. A. Reed, Observation of the linear Stark effect in a single acceptor in Si. *Phys. Rev. Lett.* **98**, 096805 (2007).
- L. E. Calvet, R. G. Wheeler, M. A. Reed, Effect of local strain on single acceptors in Si. *Phys. Rev. B* **76**, 035319 (2007).
- E. Kartheuser, S. Rodriguez, Group-theoretical study of double acceptors in semiconductors under uniaxial stress. *Phys. Rev. B* **8**, 1556–1570 (1973).
- M. Urdampilleta, A. Chatterjee, C. C. Lo, T. Kobayashi, J. Mansir, S. Barraud, A. C. Betz, S. Rogge, M. F. Gonzalez-Zalba, J. J. L. Morton, Charge dynamics and spin blockade in a hybrid double quantum dot in silicon. *Phys. Rev. X* **5**, 031024 (2015).
- M. D. Schroer, M. Jung, K. D. Petersson, J. R. Petta, Radio frequency charge parity meter. *Phys. Rev. Lett.* **109**, 166804 (2012).
- K. D. Petersson, L. W. McFaul, M. D. Schroer, M. Jung, J. M. Taylor, A. A. Houck, J. R. Petta, *Nature* **490**, 380–383 (2012).
- G. L. Bir, E. I. Butikov, G. E. Pikus, Spin and combined resonance on acceptor centres in Ge and Si type crystals—II: The effect of the electrical field and relaxation time. *J. Phys. Chem. Solids* **24**, 1475–1486 (1963).
- V. Srinivasa, K. C. Nowack, M. Shafiei, L. M. K. Vandersypen, J. M. Taylor, Simultaneous spin-charge relaxation in double quantum dots. *Phys. Rev. Lett.* **110**, 196803 (2013).
- C. H. Yang, A. Rossi, R. Ruskov, N. S. Lai, F. A. Mohiyaddin, S. Lee, C. Tahan, G. Klimeck, A. Morello, A. S. Dzurak, Spin-valley lifetimes in a silicon quantum dot with tunable valley splitting. *Nat. Commun.* **4**, 2069 (2013).
- D. V. Bulaev, D. Loss, Spin relaxation and decoherence of holes in quantum dots. *Phys. Rev. Lett.* **95**, 076805 (2005).
- P. Stano, J. Fabian, Orbital and spin relaxation in single and coupled quantum dots. *Phys. Rev. B* **74**, 045320 (2006).
- G. I. Bir, E. I. Butikov, G. E. Pikus, Spin and combined resonance on acceptor centres in Ge and Si type crystals—I: Paramagnetic resonance in strained and unstrained crystals. *J. Phys. Chem. Solids* **24**, 1467–1474 (1963).

43. R. Winkler, *Spin-orbit Coupling Effects in Two-Dimensional Electron and Hole Systems* (Springer-Verlag, Berlin Heidelberg, 2003).
44. A. Köpf, K. Lassmann, Linear Stark and nonlinear Zeeman coupling to the ground state of effective mass acceptors in silicon. *Phys. Rev. Lett.* **69**, 1580–1583 (1992).
45. A. R. Stegner, H. Tezuka, T. Andlauer, M. Stutzmann, M. L. W. Thewalt, M. S. Brandt, K. M. Itoh, Isotope effect on electron paramagnetic resonance of boron acceptors in silicon. *Phys. Rev. B* **82**, 115213 (2010).
46. F. H. L. Koppens, C. Buizert, K. J. Tielrooij, I. T. Vink, K. C. Nowack, T. Meunier, L. P. Kouwenhoven, L. M. K. Vandersypen, Driven coherent oscillations of a single electron spin in a quantum dot. *Nature* **442**, 766–771 (2006).
47. S. J. Hile, M. G. House, E. Peretz, J. Verduijn, D. Widmann, T. Kobayashi, S. Rogge, M. Y. Simmons, Radio frequency reflectometry and charge sensing of a precision placed donor in silicon. *Appl. Phys. Lett.* **107**, 093504 (2015).
48. D. Schechter, Theory of shallow acceptor states in Si and Ge. *J. Phys. Chem. Solids* **23**, 237–247 (1962).
49. A. K. Ramdas, S. Rodriguez, Spectroscopy of the solid-state analogues of the hydrogen atom: Donors and acceptors in semiconductors. *Rep. Prog. Phys.* **44**, 1297 (1981).
50. G. D. J. Smit, S. Rogge, J. Caro, T. M. Klapwijk, Group-theoretical analysis of double acceptors in a magnetic field: Identification of the  $\text{Si:B}^+$  ground state. *Phys. Rev. B* **69**, 085211 (2004).
51. A. K. Bhattacharjee, S. Rodriguez, Group-theoretical study of the Zeeman effect of acceptors in silicon and germanium. *Phys. Rev. B* **6**, 3836 (1972).

**Acknowledgments:** The device has been designed and fabricated by the TOLOP Project partners. **Funding:** This work was supported by the ARC Centre of Excellence for Quantum Computation and Communication Technology (CE110001027) and the ARC Discovery Project (DP120101825). **Author contributions:** J.v.d.H., T.K., and S.R. designed the experiments. J.v.d.H. carried out the experiments and analyzed the data, with input from T.K., M.G.H., J.S., and S.R. The transistor was provided by S.B. and R.L. All authors discussed the results. J.v.d.H. wrote the manuscript with contributions from all authors. **Competing interests:** M.Y.S. is the Director of Silicon Quantum Computing Pty Ltd. and the editor-in-chief of Nature Partner Journals (NPJ) Quantum Information and receives financial benefits from the position. The other authors declare that they have no competing interests. **Data and materials availability:** All data needed to evaluate the conclusions in the paper are present in the paper and/or the Supplementary Materials. Additional data related to this paper may be requested from the authors.

Submitted 18 April 2018

Accepted 7 November 2018

Published 7 December 2018

10.1126/sciadv.aat9199

**Citation:** J. van der Heijden, T. Kobayashi, M. G. House, J. Salfi, S. Barraud, R. Laviéville, M. Y. Simmons, S. Rogge, Readout and control of the spin-orbit states of two coupled acceptor atoms in a silicon transistor. *Sci. Adv.* **4**, eaat9199 (2018).